RESEARCH ARTICLE

Bifurcation and Stability Analysis in a Spatially Fractional-Order Diffusive Mussel-Algae Model

Dasen Lin[1] **and Ahmadjan Muhammadhaji**[1,*]

[1] College of Mathematics and System Sciences, Xinjiang University, Urumqi 830017, China

Abstract

This study elucidates the ramifications of integrating a spatial fractional-order derivative into a diffusive mussel-algae model. While the formation in such models of patterns such as Turing instability, Hopf bifurcation, and Turing-Hopf bifurcation has been extensively scrutinized in prior investigations, the impact of spatial fractional-order derivatives remains largely unknown. Beyond its ecological significance, the fractional diffusion operator is of interest because it elicits novel and nontrivial pattern formations, particularly those emerging from Turing-Hopf bifurcations. Our core objective is to dissect how spatial fractional-order derivatives modulate the spatiotemporal dynamics of a system's solutions. To characterize this degenerate bifurcation within an anomalous diffusion framework, we employ weakly nonlinear analysis to derive the corresponding amplitude equations at the Turing-Hopf bifurcation threshold. Furthermore, a systematic analysis of these amplitude equations under appropriate parametric conditions reveals a rich repertoire of spatiotemporal dynamical behaviors.

Keywords: Turing-Hopf bifurcation, fractional-order model, anomalous superdiffusion, amplitude equation.

1 Introduction

Building on Turing's foundational seminal work [1], substantial theoretical advancements have been attained in the investigation of diffusive systems, with particular emphasis on reaction-diffusion paradigms. Turing revealed that diffusion can initiate a fundamental mechanism underlying spatial pattern formation [2–4], a phenomenon that continues to galvanize extensive scholarly inquiry across diverse disciplinary domains, as corroborated by seminal contributions [5–7]. Moreover, the exploration of the Hopf bifurcation [10, 15, 16], Turing bifurcation [8, 9, 11–13], and stability properties of steady-state configurations remain a major focus of contemporary research.

A notable recent advancement lies in the characterization of the Turing-Hopf bifurcation, which is a codimension-two bifurcation. This dynamical phenomenon emerges within specific reaction-diffusion frameworks and is delineated by the onset of spatiotemporal periodic oscillations arising from the concurrent initiation of Hopf and Turing bifurcations. The analytical investigation of this pivotal dynamical regime constitutes a topic of substantial scholarly interest [14–16], with empirical support for spatially self-organized pattern formation in mussel bed ecosystems further motivating this line

Submitted: 23 April 2026
Accepted: 15 June 2026
Published: 28 June 2026

Vol. 2, **No.** 2, 2026.
10.62762/JNDA.2026.807630

***Corresponding author:**
✉ Ahmadjan Muhammadhaji
ahmatjanam@aliyun.com

Citation
Lin, D., & Muhammadhaji, A. (2026). Bifurcation and Stability Analysis in a Spatially Fractional-Order Diffusive Mussel-Algae Model. *Journal of Nonlinear Dynamics and Applications*, 2(2), 127–142.

© 2026 ICCK (Institute of Central Computation and Knowledge)

of inquiry [17].

This study employs the mussel-algae model as a paradigmatic framework. The model, whose ecological structure was established in the foundational works on intertidal mussel bed dynamics [21, 23], takes the following form as adapted by Rovinsky and Menzinger [18] to incorporate Turing-Hopf interaction mechanisms:

$$\begin{cases} \dfrac{\partial M(t,x)}{\partial t} = ecM(t,x)A(t,x) - \dfrac{dkM(t,x)}{k+M(t,x)} \\ \qquad\qquad - D\Delta M(t,x), \\ \dfrac{\partial A(t,x)}{\partial t} = (a_{\text{up}} - A(t,x))\,\rho - \dfrac{c}{h}A(t,x)M(t,x) \\ \qquad\qquad - V\nabla_y A(t,x). \end{cases} \tag{1}$$

This formulation reveals the intrinsic pattern-forming processes in which the algae function as the primary nutritional resource for mussels. Song et al. [19] subsequently refined the model by introducing a constant advection term for the algae to emulate the environmental conditions in intertidal flat ecosystems. Subsequent scholarly endeavors have extensively investigated the regulatory factors governing the propagation dynamics of mussel-algae bed systems; for example, the effects of reduced food concentration were studied by Song et al. [20]. Mathematically, this ecological interaction is distinguished by its dynamical intricacy, manifesting phenomena from wave pattern generation [21] to nonlinear pattern stability under stochastic perturbations [22], with additional illustrative cases documented in [19, 22, 23].

A 2020 investigation by Djilali et al. [27] considered the following temporal-fractional variant of the mussel-algae model:

$$\begin{cases} \dfrac{\partial^\delta M(t,x)}{\partial t^\delta} = ecM(t,x)A(t,x) - \dfrac{dkM(t,x)}{k+M(t,x)} \\ \qquad\qquad + d_1\nabla^2 M(t,x), \\ \dfrac{\partial^\delta A(t,x)}{\partial t^\delta} = (a_{\text{up}} - A(t,x))\,\rho - \dfrac{c}{h}A(t,x)M(t,x) \\ \qquad\qquad + d_2\nabla^2 A(t,x). \end{cases} \tag{2}$$

Here, $M(t,x)$ and $A(t,x)$ represent the mussel and algal densities, respectively. Parameter e denotes the conversion efficiency of algal biomass to mussel biomass, c signifies the algal consumption rate by mussels, d is the maximum per capita mussel mortality rate, k represents the mussel saturation constant, a_{up} defines the uniform algae concentration in the upper sea stratum, and ρ quantifies the reciprocal exchange rate between sea strata. Finally, d_1 and d_2 are the spatial diffusion coefficients for mussels and algae, respectively.

Like the prior work cited above, this study is inherently limited by its adherence to conventional diffusion formulations. Nevertheless, its analysis of Turing-Hopf bifurcations within the theoretical framework of classical reaction-diffusion systems using the mussel-algae diffusion model yields the first theoretical demonstration of higher-codimension bifurcations in systems incorporating fractional temporal derivatives, as corroborated by numerical simulations.

Conventional Fickian diffusion is typified by a mean-squared displacement that scales linearly with time as $\langle x^2(t)\rangle \propto t$. However, a growing body of empirical and theoretical evidence [25, 26] has revealed that diffusion is frequently anomalous over extended temporal scales. In anomalous diffusion, the displacement follows $\langle x^2(t)\rangle \propto t^\xi$, where ξ is the diffusion exponent. Exponents within the ranges $0 < \xi < 1$, $\xi = 1$, $1 < \xi < 2$, and $\xi = 2$ correspond respectively to subdiffusion, normal diffusion, Lévy superdiffusion, and ballistic diffusion [24, 27]. Such anomalous diffusion processes are widely observed in natural systems [28–30], and differential equations incorporating fractional orders are increasingly recognized as more accurate mathematical representations of anomalous diffusion and complex system dynamics [31]. For example, studies [32, 33, 39] indicate that animal movement observed at larger spatial or temporal scales aligns with Lévy walk models. Consequently, the corresponding biological models should be described using anomalously diffusive systems. In recent years, interest in predator-prey systems that exhibit superdiffusion has grown. For instance, Cheng and Yuan [34] investigated the spreading properties in a prey-predator system where diffusion was modeled using a fractional Laplacian operator, whereas Bendahmane et al. [35] introduced fractional-in-space operators into a Lotka-Volterra competitive model to characterize population superdiffusion and analyze its influence on pattern formation, presenting the associated Turing patterns. Prior studies on fractional reaction-diffusion systems have further highlighted the importance of nonlocal diffusion and memory effects in pattern formation [36–38]. These works demonstrate that

stability criteria and bifurcation mechanisms in fractional activator-inhibitor and Brusselator-type systems share structural analogies with those in ecological reaction-diffusion models, motivating the incorporation of fractional operators into the present mussel-algae framework. This body of work strongly motivates the incorporation of anomalous diffusion mechanisms into reaction-diffusion system analysis. Therefore, omitting the fractional operator would amount to assuming normal diffusion, which contradicts field observations of Lévy-flight-like movement inthese ecosystems.

Consequently, this study extends system (2) to a two-dimensional spatial domain, investigating the following superdiffusive mussel-algae system incorporating spatial fractional-order derivatives:

$$\begin{cases} \frac{\partial M(x,y,t)}{\partial t} = ecMA - \frac{dkM}{k+M} + d_1\nabla^\theta M, & (x,y)\in\Omega, \\ \frac{\partial A(x,y,t)}{\partial t} = (a_{\text{up}} - A)\,\rho - \frac{c}{h}AM + d_2\nabla^\theta A, & (x,y)\in\Omega, t>0, \\ M(x,y,t) = A(x,y,t) = 0, & (x,y)\in\mathbb{R}^2\setminus\Omega, \quad t>0, \\ M(x,y,0) = M_0 > 0, \quad A(x,y,0) = A_0 > 0, & (x,y)\in\Omega, \end{cases} \tag{3}$$

where ∇^θ $(1<\theta<2)$ denotes a spatial fractional operator, $(x,y)\in\Omega$ (a bounded open domain in $\mathbb{R}^2$). The anomalous diffusion operator ∇^θ is defined via the Riesz fractional derivative [30, 31]:

$$\begin{aligned} \nabla^\theta M &= \frac{\partial^\theta M}{\partial|x|^\theta} + \frac{\partial^\theta M}{\partial|y|^\theta} \\ &= -\frac{1}{2\cos(\pi\theta/2)}\left({}_{\text{RL}}D^\theta_{-\infty,x}M + {}_{\text{RL}}D^\theta_{x,+\infty}M\right) \\ &\quad - \frac{1}{2\cos(\pi\theta/2)}\left({}_{\text{RL}}D^\theta_{-\infty,y}M + {}_{\text{RL}}D^\theta_{y,+\infty}M\right), \end{aligned}$$

The constituent Riemann-Liouville derivatives are defined as:

$${}_{\text{RL}}D^\theta_{-\infty,x}M = \frac{1}{\Gamma(2-\theta)}\frac{\partial^2}{\partial x^2}\int_{-\infty}^{x}(x-s)^{1-\theta}M(s,y,t)\mathrm{d}s,$$
$${}_{\text{RL}}D^\theta_{x,+\infty}M = \frac{1}{\Gamma(2-\theta)}\frac{\partial^2}{\partial x^2}\int_{x}^{+\infty}(s-x)^{1-\theta}M(s,y,t)\mathrm{d}s,$$

where $\Gamma(\cdot)$ is the Gamma function. The definitions for ${}_{\text{RL}}D^\theta_{-\infty,y}M$ and ${}_{\text{RL}}D^\theta_{y,+\infty}M$ follow analogously.

2 Turing-Hopf bifurcation analysis

In this section, we analyze the existence of the Turing-Hopf bifurcation. To reduce the number of parameters, we employ the following variable transformation:

$$\tilde{x} = x\sqrt[\theta]{d},\ \tilde{y} = y\sqrt[\theta]{d},\ \tilde{t} = dt,\ \tilde{M} = \frac{M}{k},\ \tilde{A} = \frac{A}{a_{up}},$$

and introduce the dimensionless quantities:

$$\beta = \frac{eca_{up}}{d}, \quad m = \frac{\rho h}{ck}, \quad \alpha = \frac{ck}{dh}.$$

Upon omitting tildes for notational simplicity, system (3) transforms into

$$\begin{cases} \dfrac{\partial M}{\partial t} = \beta MA - \dfrac{M}{1+M} + d_1\nabla^\theta M, \\ \dfrac{\partial A}{\partial t} = (1-A)m\alpha - \alpha AM + d_2\nabla^\theta A. \end{cases} \tag{4}$$

As established in [27], the system admits the following homogeneous steady-states
(i) The semi-trivial steady state $(0,1)$, corresponding to mussel extinction, which exists unconditionally.
(ii) The interior homogeneous steady state $E^* = (M^*, A^*)$ representing species coexistence, where

$$M^* = \frac{m(\beta-1)}{1-m\beta}, \quad A^* = \frac{1-m\beta}{\beta(1-m)},$$

whose existence requires satisfaction of either condition

$$(A_1): \frac{1}{m} < \beta < 1.$$
$$(A_2): 1 < \beta < \frac{1}{m}.$$

To investigate the stability properties of the interior equilibrium (M^*, A^*), a coordinate transformation is applied to shift this steady state to the origin:

$$U(t) = \begin{pmatrix} \bar{M}(t) \\ \bar{A}(t) \end{pmatrix} = \begin{pmatrix} M(t) - M^* \\ A(t) - A^* \end{pmatrix}.$$

For notational simplicity, we retain $M(t)$ and $A(t)$ to denote the transformed variables. The system (4) is consequently reformulated as

$$U_t = J_0\begin{pmatrix} M \\ A \end{pmatrix} + \begin{pmatrix} f(M,A) \\ g(M,A) \end{pmatrix} + D\nabla^\theta U, \tag{5}$$

where the diffusion matrix D and Jacobian J_0 are defined as:

$$D = \begin{pmatrix} d_1 & 0 \\ 0 & d_2 \end{pmatrix},$$
$$J_0 = \begin{pmatrix} \beta A^*(1-\beta A^*) & \beta M^* \\ -\alpha A^* & -\alpha(m+M^*) \end{pmatrix} \triangleq \begin{pmatrix} j_{11} & j_{12} \\ j_{21} & j_{22} \end{pmatrix},$$

with the nonlinear components given by

$$f(M,A) = (\beta A^*)^3M^2 + \beta MA - (\beta A^*)^4M^3 + \cdots,$$
$$g(M,A) = -\alpha MA + \cdots.$$

The corresponding linearized system takes the form

$$\begin{pmatrix} \frac{\partial M}{\partial t} \\ \frac{\partial A}{\partial t} \end{pmatrix} = D \begin{pmatrix} \nabla^\theta M \\ \nabla^\theta A \end{pmatrix} + J_0 \begin{pmatrix} M \\ A \end{pmatrix}. \tag{6}$$

To examine the linear stability of (M^*, A^*), we consider solutions of the form:

$$\begin{pmatrix} M \\ A \end{pmatrix} = \begin{pmatrix} c_1 \\ c_2 \end{pmatrix} \exp(\lambda t + ik \cdot x). \tag{7}$$

The characteristic equation for (6) generates a sequence of quadratic equations

$$\Delta_k = \lambda^2 - T_k \lambda + D_k = 0, \quad \forall k \in \mathbb{N}_0, \tag{8}$$

where the trace T_k and determinant D_k are given by

$$T_k = \beta A^*(1-\beta A^*) - \alpha(m+M^*) - (d_1+d_2)k^\theta, \tag{9}$$

$$\begin{aligned} D_k = {} & \alpha\beta A^*(\beta A^*-1)(m+M^*) + \alpha\beta A^* M^* \\ & - \left[d_2\beta A^*(1-\beta A^*) - d_1\alpha(m+M^*)\right]k^\theta \\ & + d_1 d_2 k^{2\theta}. \end{aligned} \tag{10}$$

Under condition (A_1), it readily follows that $T_k < 0$ and $D_k > 0$. This implies that both roots of equation (8) possess negative real parts. Consequently, for any α, the positive equilibrium point E^* is asymptotically stable. For the subsequent analysis, we assume the validity of condition (A_2).

A bifurcation is classified as Turing-Hopf type when the following conditions are simultaneously satisfied [40]:

I. There exists a nonnegative integer k such that $\Delta_k = 0$ admits a pair of purely imaginary roots.

II. There exists a distinct positive integer $n \neq k$ such that $\Delta_n = 0$ possesses a simple zero root.

III. No other roots of the characteristic equation (8) have zero real parts.

IV. The transversality condition is fulfilled.

Theorem 1. Let E^* be the positive equilibrium of system (4). Taking α as the bifurcation parameter, we define the maximum wavenumber

$$\begin{aligned} k_{\max} &= \max\left\{k \in \mathbb{N}_0 \,\middle|\, \beta A^*(1-\beta A^*) - d_1 k^\theta > 0\right\} \\ &= \left\lfloor \left(\frac{\beta A^*(1-\beta A^*)}{d_1}\right)^{1/\theta} \right\rfloor. \end{aligned}$$

Then, in the (α, d_2) parameter plane, the bifurcation phenomena of system (4) near E^* are described as follows:

(1).Hopf bifurcation

For each integer k with $0 \le k \le k_{\max}$, there exists a Hopf bifurcation curve

$$\begin{aligned} \mathcal{L}_{Hk} : \; d_2 &= d_{2H}(\alpha, k) \\ &= -\frac{m+M^*}{k^\theta}\alpha + \frac{\beta A^*(1-\beta A^*) - d_1 k^\theta}{k^\theta}, \; \alpha < \alpha_k^*, \end{aligned}$$

where $\alpha_k^* = \dfrac{\beta A^*(1-\beta A^*) - d_1 k^\theta}{\beta M^* A^*}$. As the parameter (α, d_2) crosses $\mathcal{L}_{Hk}$ transversely, system (4) undergoes a Hopf bifurcation at E^*, giving rise to spatially nonhomogeneous periodic solutions.

(2).Turing bifurcation

For each integer k with $1 \le k \le k_{\max}$, there exists a Turing bifurcation curve

$$\begin{aligned} \mathcal{L}_{Tk} : \; \alpha &= \alpha_T(d_2, k) \\ &= \frac{\left[\beta A^*(1-\beta A^*)k^\theta - d_1 k^{2\theta}\right] d_2}{\beta A^*(\beta A^*-1)(m+M^*) + \beta M^* A^* + (m+M^*)d_1 k^\theta}. \end{aligned}$$

When the parameter (α, d_2) crosses $\mathcal{L}_{Tk}$ transversely and $T_k \neq 0$, system (4) undergoes a Turing bifurcation at E^*, leading to the formation of spatial patterns.

(3).Turing-Hopf bifurcation

Define the slope function of the curve $\mathcal{L}_{Tk}$ as

$$\mathcal{S}(k) = \frac{\beta A^*(1-\beta A^*)k^\theta - d_1 k^{2\theta}}{\beta A^*(\beta A^*-1)(m+M^*) + \beta M^* A^* + (m+M^*)d_1 k^\theta}, \quad 1 \le k \le k_{\max},$$

and let $k^c \in [1, k_{\max}]$ be the wavenumber that maximizes $\mathcal{S}(k)$. Then, the Hopf bifurcation curve $\mathcal{L}_{H0}$ and the Turing bifurcation curve $\mathcal{L}_{Tk^c}$ intersect transversely at the parameter point

$$(d_2^*, \alpha^*) = \left(d_{2H}(\alpha^*, 0), \alpha_T(d_2^*, k^c)\right).$$

When $(\alpha, d_2) = (\alpha^*, d_2^*)$, system (4) undergoes a Turing-Hopf bifurcation at E^*, where Hopf instability and Turing instability occur simultaneously.

Proof: A Hopf bifurcation occurs if and only if $T_k = 0$ and $D_k > 0$. Solving $T_k = 0$ from (9) and (10) gives the Hopf curve (11), and solving $D_k = 0$ yields the Turing curve (12). Where

$$d_2 = d_{2H}(\alpha, k) = -\frac{m+M^*}{k^\theta}\alpha + \frac{\beta A^*(1-\beta A^*) - d_1 k^\theta}{k^\theta}, \tag{11}$$

while $D_k = 0$ corresponds to

$$\begin{aligned} d_2 &= d_{2T}(\alpha, k) \\ &= \frac{\beta A^*(\beta A^*-1)(m+M^*) + \beta M^* A^* + (m+M^*)d_1 k^\theta}{\beta A^*(1-\beta A^*)k^\theta - d_1 k^{2\theta}}\alpha. \end{aligned} \tag{12}$$

The intersection of the lines $d_2 = d_{2H}(\alpha, k)$ and $d_2 = d_{2T}(\alpha, k)$, obtained from (11) and (12), yields

$$\alpha = \tilde{\alpha}_k = \frac{\beta A^*(1-\beta A^*) - d_1 k^\theta}{\beta M^* A^*}. \tag{13}$$

Solving equation (11) for α provides the expression

$$\begin{aligned} \alpha &= \alpha_H(d_2, k) \\ &= -\frac{k^\theta}{m+M^*} d_2 + \frac{\beta A^*(1-\beta A^*) - d_1 k^\theta}{m+M^*}, \\ k &= 1, 2, \ldots, k_{\max}, \end{aligned}$$

where

$$k_{\max} = \max\left\{ k \in \mathbb{N}_0 \mid \beta A^*(1-\beta A^*) - d_1 k^\theta > 0 \right\}.$$

For a fixed wavenumber $k \in [0, k_{\max}]$, if $\alpha < \alpha_k^*$ and $d_2 = d_{2H}(\alpha, k)$, then equation (8) possesses a purely imaginary root pair $\pm i\omega$ ($\omega = \sqrt{D_k} > 0$). To verify the transversality condition for the Hopf bifurcation, we treat α as the bifurcation parameter and denote the root of Eq. (8) by $\lambda(\alpha)$. Eq. (8) with respect to α yields

$$2\lambda \frac{\mathrm{d}\lambda}{\mathrm{d}\alpha} - \left(\frac{\mathrm{d}T_k}{\mathrm{d}\alpha}\lambda + T_k \frac{\mathrm{d}\lambda}{\mathrm{d}\alpha} \right) + \frac{\mathrm{d}D_k}{\mathrm{d}\alpha} = 0. \tag{14}$$

Evaluating at the Hopf threshold $\alpha = \alpha_H(d_2, k)$ where $T_k = 0$ and $\lambda = \pm i\omega$, we obtain

$$\left. \frac{d\,\mathrm{Re}\,\lambda(\alpha)}{d\alpha} \right|_{\alpha=\alpha_H(d_2,k)} = -\frac{m+M^*}{2} < 0. \tag{15}$$

Based on equations (11), (12), and (15), we define lines in the α-d_2 parameter plane:

$$\mathcal{L}_{Hk} : d_2 = d_{2H}(\alpha, k), \quad \alpha < \alpha^*, \quad k = 1, 2, \ldots, k_{\max}. \tag{16}$$

Along each line $\mathcal{L}_{Hk}$, system (4) undergoes a Hopf bifurcation near the equilibrium E^*, giving rise to spatially inhomogeneous solutions.

The line $\mathcal{L}_{H0}$ ($k = 0$) corresponds to the case without diffusion. The stability conditions for the equilibrium E^* in the absence of diffusion are

$$\begin{aligned} T_0 &= \frac{m(1-m\beta)(\beta-1)}{(1-m)^2} + \frac{\alpha m\beta(m-1)}{1-m\beta} < 0, \\ D_0 &= \frac{\alpha m(1-m\beta)(\beta-1)}{1-m} > 0. \end{aligned}$$

Consequently, the equilibrium (M^*, A^*) remains stable provided $\alpha > \frac{\beta A^*(1-\beta A^*)}{m+M^*}$, but becomes unstable when $\alpha < \frac{\beta A^*(1-\beta A^*)}{m+M^*}$.

We now investigate the Turing bifurcation. To analyze this instability, equations (11) and (12) are reformulated as:

$$\begin{aligned} \alpha &= \alpha_H(d_2, k) \\ &= -\frac{k^\theta}{m+M^*} d_2 + \frac{\beta A^*(1-\beta A^*) - d_1 k^\theta}{m+M^*}, \end{aligned} \tag{17}$$

and

$$\begin{aligned} \alpha &= \alpha_T(d_2, k) \\ &= \frac{\left[\beta A^*(1-\beta A^*)k^\theta - d_1 k^{2\theta}\right] d_2}{\beta A^*(\beta A^*-1)(m+M^*) + \beta M^* A^* + (m+M^*) d_1 k^\theta}. \end{aligned} \tag{18}$$

In the α-d_2 parameter plane, the curve defined by $D_k = 0$ constitutes the Turing bifurcation curve, denoted $\mathcal{L}_{Tk}$ for $k = 1, 2, \ldots, k_{\max}$. Considering α as the bifurcation parameter and letting $\lambda(\alpha)$ represent the root of Eq. (8), we obtain:

$$\left. \frac{d\,\mathrm{Re}\,\lambda(\alpha)}{d\alpha} \right|_{\alpha=\alpha_T(d_2,k}} = \frac{\beta A^*(\beta A^*-1)(m+M^*) + \beta M^* A^* - (m+M^*) d_1 k^\theta}{T_k} \neq 0, \tag{19}$$

verifying that system (4) undergoes a Turing bifurcation near equilibrium (M^*, A^*) along $\mathcal{L}_{Tk}$.

For wavenumbers $k \in [0, k_{\max}]$, the relations $-(m+M^*) < 0$, $-\frac{\beta A^*(1-\beta A^*) - d_1 k^\theta}{m+M^*} \leq \frac{\beta A^*(1-\beta A^*)}{m+M^*}$, and Eq. (18) imply that all Hopf bifurcation lines $\mathcal{L}_{Hk}$ ($1 \leq k \leq k_{\max}$) lie below $\mathcal{L}_{H0}$. The slope of the Turing bifurcation line $\mathcal{L}_{Tk}$ is given by:

$$\mathcal{S}(k) = \frac{\beta A^*(1-\beta A^*)k^\theta - d_1 k^{2\theta}}{\beta A^*(\beta A^*-1)(m+M^*) + \beta M^* A^* + (m+M^*) d_1 k^\theta}.$$

This slope exhibits distinct behavior:

$$\mathcal{S}(k) = \begin{cases} > 0, & 1 \leq k \leq k_{\max} = \left\lfloor \left(\frac{\beta A^*(1-\beta A^*)}{d_1} \right)^{1/\theta} \right\rfloor, \\ < 0, & k > k_{\max} = \left\lfloor \left(\frac{\beta A^*(1-\beta A^*)}{d_1} \right)^{1/\theta} \right\rfloor, \end{cases} \tag{20}$$

where $\lfloor \cdot \rfloor$ denotes the floor function. When $k > k_{\max}$, the Turing bifurcation curve $\mathcal{L}_{Tk}$ does not intersect the Hopf bifurcation curve $\mathcal{L}_{H0}$. Consequently, system (4) does not undergo a Turing-Hopf bifurcation and remains stable along $\mathcal{L}_{H0}$. We therefore restrict our analysis to $1 \leq k \leq k_{\max}$.

Define the auxiliary function:

$$\mathcal{F}(n) = \frac{\beta A^*(1-\beta A^*)n - d_1 n^2}{\beta A^*(\beta A^*-1)(m+M^*) + \beta M^* A^* + (m+M^*) d_1 n}. \tag{21}$$

This function satisfies $\mathcal{F}'(n) \geq 0$ for $n \leq \tilde{n}$ and $\mathcal{F}'(n) < 0$ for $n > \tilde{n}$, with critical point:

$$\tilde{n} = -\frac{\beta A^*}{d_1(m+M^*)}\left((\beta A^*(m+M^*)-m) - \sqrt{M^*\left(\beta A^*(m+M^*)-m\right)}\right).$$

The critical wavenumber k^c is then determined as:

$$k^c = \begin{cases} \left\lfloor \tilde{n}^{1/\theta} \right\rfloor, & \mathcal{S}\left(\left\lfloor \tilde{n}^{1/\theta} \right\rfloor + 1\right) \leq \mathcal{S}\left(\left\lfloor \tilde{n}^{1/\theta} \right\rfloor\right), \\ \left\lfloor \tilde{n}^{1/\theta} \right\rfloor + 1, & \mathcal{S}\left(\left\lfloor \tilde{n}^{1/\theta} \right\rfloor\right) < \mathcal{S}\left(\left\lfloor \tilde{n}^{1/\theta} \right\rfloor + 1\right). \end{cases} \tag{22}$$

For $k^c \in [1, k_{\max}]$, the wavenumber maximizing $\mathcal{S}(k)$, the Hopf bifurcation curve $\mathcal{L}_{H0}$ intersects the Turing bifurcation curve $\mathcal{L}_{Tk^c}$ transversely at (d_2^*, α^*), thereby partitioning the stability region in the parameter plane.

Remark 1. Under the parameter configuration $\beta = 2.5$, $m = 0.3$, and $d_1 = 0.15$, the critical wavenumber is computed as $k^c = k_{\max} = 1$, with corresponding bifurcation values $\mathcal{L}_{H0} = 0.1093$ and $\mathcal{S}(k) = 0.1672$. The intersection of the Hopf bifurcation curve $\mathcal{L}_{H0}$ and Turing bifurcation curve $\mathcal{L}_{T1}$ occurs at the critical point $(\alpha^*, d_2^*) = (0.1093, 0.6535)$. In proximity to the positive equilibrium $(1.1538, 0.2133)$, system (4) undergoes a Turing-Hopf bifurcation, as illustrated in Figure 1.

Figure 1 illustration of the parameter plane, divided into four distinct regions: R_1 (stable), R_2 (Turing instability), R_3 (Hopf instability), and R_4 (simultaneous Turing-Hopf instability).

3 Weakly nonlinear analysis

For theoretical analysis, periodic boundary conditions are first imposed on a finite domain; the limit of an infinite system size is subsequently considered to render boundary effects negligible, yielding the standard amplitude equations. As established in the preceding section, this approach yields the Turing-Hopf bifurcation point. We now derive the amplitude equations at this bifurcation point using weakly nonlinear analysis. Furthermore, our analysis reveals an interaction between a Turing mode $T\,(k^c, 0)$, characterized by wavenumber k^c, and a homogeneous Hopf mode $H\,(0, \omega_c)$, characterized by frequency ω_c. Consequently, the solution to Eq. (6) is expanded as:

$$U = \varepsilon U^{(1)} + \varepsilon^2 U^{(2)} + \varepsilon^3 U^{(3)} + \cdots, \tag{23}$$

where

$$U^{(1)} = \sum_j \left[Z_j \exp\left(ik_j \cdot x\right) + B\exp\left(i\omega_c t\right)\right] + \text{c.c.},$$

with c.c. denoting the complex conjugate term (used consistently hereafter).

Introduce the slow time scale $T_2 = \varepsilon^2 t$ and expand the variables M, A, and the bifurcation parameters α and d_2 as:

$$\begin{aligned} \begin{pmatrix} M \\ A \end{pmatrix} &= \varepsilon \begin{pmatrix} M_1 \\ A_1 \end{pmatrix} + \varepsilon^2 \begin{pmatrix} M_2 \\ A_2 \end{pmatrix} + \varepsilon^3 \begin{pmatrix} M_3 \\ A_3 \end{pmatrix} + \cdots, \\ d_2 &= d_2^* + d^{(2)}\varepsilon^2, \\ \alpha &= \alpha^* + \alpha^{(2)}\varepsilon^2. \end{aligned} \tag{24}$$

Treating the Turing mode amplitudes Z_j and the Hopf mode amplitude B as slowly varying quantities implies:

$$\begin{aligned} \frac{\partial Z_j}{\partial t} &= \varepsilon^2 \frac{\partial Z_j}{\partial T_2} + \mathcal{O}\left(\varepsilon^3\right), \\ \frac{\partial B}{\partial t} &= \varepsilon^2 \frac{\partial B}{\partial T_2} + \mathcal{O}\left(\varepsilon^3\right). \end{aligned} \tag{25}$$

Substituting expansion (24) into system (6) and collecting terms of order $\varepsilon^j (j = 1, 2, 3)$ yields the following hierarchy of equations:

$$\begin{aligned} \mathcal{O}(\varepsilon): &\quad L_c\left(k^\theta\right)\begin{pmatrix} M_1 \\ A_1 \end{pmatrix} = 0, \\ \mathcal{O}\left(\varepsilon^2\right): &\quad L_c\left(k^\theta\right)\begin{pmatrix} M_2 \\ A_2 \end{pmatrix} = -\begin{pmatrix} f_{\varepsilon^2} \\ g_{\varepsilon^2} \end{pmatrix}, \\ \mathcal{O}\left(\varepsilon^3\right): &\quad L_c\left(k^\theta\right)\begin{pmatrix} M_3 \\ A_3 \end{pmatrix} = \frac{\partial}{\partial T_2}\begin{pmatrix} M_1 \\ A_1 \end{pmatrix} - \mathcal{N}\begin{pmatrix} M_1 \\ A_1 \end{pmatrix} - \begin{pmatrix} f_{\varepsilon^3} \\ g_{\varepsilon^3} \end{pmatrix}, \end{aligned}$$

where the linearized system (6) is denoted by

$$\begin{aligned} U_t &= \left[L_c\left(k^\theta\right) + \varepsilon^2 \mathcal{N}\right] U, \\ \mathcal{N} &= \begin{pmatrix} 0 & 0 \\ -\alpha^{(2)} A^* & -\alpha^{(2)}(m+M^*) + d_2^{(2)}\nabla^\theta \end{pmatrix}, \\ L_c\left(k^\theta\right) &= \begin{pmatrix} \beta A^*(1-\beta A^*) - d_1 k^\theta & \beta M^* \\ -\alpha^* A^* & -\alpha^*(m+M^*) - d_2^* k^\theta \end{pmatrix}, \\ \begin{pmatrix} f_{\varepsilon^2} \\ g_{\varepsilon^2} \end{pmatrix} &= \begin{pmatrix} (\beta A^*)^3 M_1^2 + \beta M_1 A_1 \\ -\alpha M_1 A_1 \end{pmatrix}, \\ \begin{pmatrix} f_{\varepsilon^3} \\ g_{\varepsilon^3} \end{pmatrix} &= \begin{pmatrix} 2(\beta A^*)^3 M_1 A_2 + \beta(M_1 A_2 + M_2 A_1) \\ -((\beta A^*)^4) M_1^3 \\ -\alpha(M_1 A_2 + M_2 A_1) \end{pmatrix}. \end{aligned}$$

The linear operator L_c satisfies the eigenvalue equations:

$$L_c\left(k^c\right)\zeta = 0, \quad L_c(0)\eta = i\omega_c \eta,$$

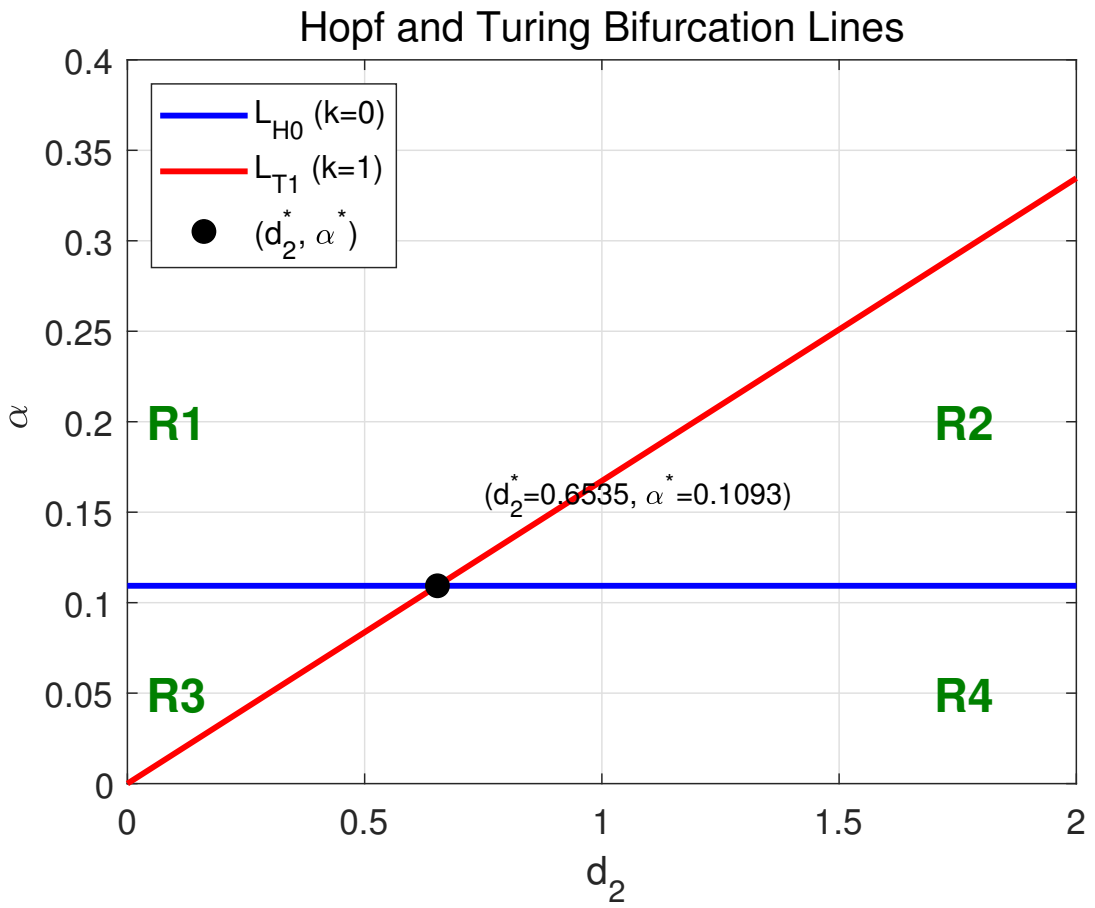

Figure 1. Bifurcation diagram of system (4) in the d_2-α plane for $k^c = 1$.

with eigenvectors given by

$$\zeta = \begin{pmatrix} \zeta_1 \\ \zeta_2 \end{pmatrix} = \begin{pmatrix} \frac{\beta M^*}{d_1 k^\theta + \beta A^*(\beta A^* - 1)} \\ 1 \end{pmatrix},$$
$$\eta = \begin{pmatrix} \eta_1 \\ \eta_2 \end{pmatrix} = \begin{pmatrix} \frac{\beta M^*}{i\omega_c + \beta A^*(\beta A^* - 1)} \\ 1 \end{pmatrix}.$$

The first-order solution is assumed to be

$$\begin{pmatrix} M_1 \\ A_1 \end{pmatrix} = \sum_{j=1}^{3} \begin{pmatrix} X_j \\ Y_j \end{pmatrix} e^{ik_j \cdot x} + \begin{pmatrix} B^M \\ B^A \end{pmatrix} e^{i\omega_c t} + \text{c.c.}, \quad (26)$$

where $|k_j|^\theta = k^c$ for $j = 1, 2, 3$. This implies the correspondence:

$$Z_j = \begin{pmatrix} X_j \\ Y_j \end{pmatrix} = qW_j, \quad B = \begin{pmatrix} B^M \\ B^A \end{pmatrix} = p\mathcal{H}.$$

Guided by the structure of the nonlinearities, the second-order solution $U^{(2)}$ is postulated to contain specific resonant modes

$$\begin{aligned} \begin{pmatrix} M_2 \\ A_2 \end{pmatrix} =& \begin{pmatrix} \mathcal{M}_0 \\ \mathcal{A}_0 \end{pmatrix} + \sum_{j=1}^{3} \left[\begin{pmatrix} \mathcal{M}_j \\ \mathcal{A}_j \end{pmatrix} e^{ik_j \cdot x} + \begin{pmatrix} \mathcal{M}_{jj} \\ \mathcal{A}_{jj} \end{pmatrix} e^{i2k_j \cdot x} \right] \\ &+ \begin{pmatrix} \mathcal{M}_H \\ \mathcal{A}_H \end{pmatrix} e^{i2\omega_c t} + \sum_{n \neq j > 0} \begin{pmatrix} \mathcal{M}_{nj} \\ \mathcal{A}_{nj} \end{pmatrix} e^{i(k_n - k_j) \cdot x} \\ &+ \begin{pmatrix} \mathcal{M}_{TH} \\ \mathcal{A}_{TH} \end{pmatrix} e^{i(k_j \cdot x + \omega_c t)} + \text{c.c.}. \end{aligned} \quad (27)$$

Substituting (27) into the $\mathcal{O}(\varepsilon^2)$ equation,

$$\begin{aligned} &\left(\beta A^*(1 - \beta A^*) + d_1 \nabla^\theta\right) M_2 + \beta M^* A_2 = -f_{\varepsilon^2}, \\ &-\alpha^* A^* M_2 + \left(-\alpha^*(m + M^*) + d_2 \nabla^\theta\right) A_2 = -g_{\varepsilon^2}, \end{aligned}$$

and equating coefficients for each mode type results

in the expressions

$$\begin{aligned}
\mathcal{M}_0 &= \mathcal{M}_{0T} + \mathcal{M}_{0H}, & \mathcal{M}_{0T} &= E_{1T}\mathcal{A}_{0T},\\
\mathcal{A}_{0T} &= E_{2T}\left|W_j\right|^2, & \mathcal{M}_{0H} &= E_{1H}\mathcal{A}_{0H},\\
\mathcal{A}_{0H} &= E_{2H}|\mathcal{H}|^2, & \mathcal{M}_j &= q_1 V_j,\\
\mathcal{M}_{12} &= E_5\mathcal{A}_{12}, & \mathcal{A}_{jj} &= E_4 W_j^2,\\
\mathcal{A}_{12} &= E_6 W_1\bar{W}_2, & \mathcal{M}_H &= E_7\mathcal{A}_H,\\
\mathcal{A}_H &= E_8\mathcal{H}^2, & \mathcal{M}_{TH} &= E_9\mathcal{A}_{TH},\\
\mathcal{A}_{TH} &= E_{10}W_j B, & \mathcal{M}_{jj} &= E_3\mathcal{A}_{jj}.
\end{aligned}$$

The coefficients E_i are defined by:

$$\begin{aligned}
E_{1T} &= \frac{b_T j_{12} - a_T\alpha^* j_{22}/\alpha}{a_T\alpha^* j_{21}/\alpha - b_T j_{11}},\\
E_{1H} &= \frac{b_H j_{12} - a_H\alpha^* j_{22}/\alpha}{a_H\alpha^* j_{21}/\alpha - b_H j_{11}},\\
E_{2T} &= -\frac{a_T}{j_{11}E_{1T} + j_{12}},\\
E_{2H} &= -\frac{a_H}{j_{11}E_{1H} + j_{12}},\\
E_3 &= \frac{a_{2T}(\alpha^* j_{22}/\alpha - d_2^*(2|k|)^\theta) - b_{2T}j_{12}}{b_{2T}(j_{11} - d_1(2|k|)^\theta) - a_{2T}\alpha^* j_{21}/\alpha},\\
E_4 &= -\frac{a_{2T}}{(j_{11} - (2|k|)^\theta)E_3 + j_{12}},\\
E_5 &= \frac{a_{3T}(\alpha^* j_{22}/\alpha - d_2^*(\sqrt{3}|k|)^\theta) - b_{3T}j_{12}}{b_{3T}(j_{11} - d_1(\sqrt{3}|k|)^\theta) - a_{3T}\alpha^* j_{21}/\alpha},\\
E_6 &= -\frac{a_{3T}}{(j_{11} - (\sqrt{3}|k|)^\theta)E_5 + j_{12}},\\
E_7 &= \frac{b_{4H}j_{12} - a_{4H}\alpha^* j_{22}/\alpha}{a_{4H}\alpha^* j_{21}/\alpha - b_{4H}j_{11}},\\
E_8 &= -\frac{a_{4H}}{j_{11}E_{1H} + j_{12}},\\
E_9 &= \frac{a_{5T}(\alpha^* j_{22}/\alpha - d_2^*|k|^\theta) - b_{5T}j_{12}}{b_{5T}(j_{11} - d_1|k|^\theta) - a_{5T}\alpha^* j_{21}/\alpha},\\
E_{10} &= -\frac{a_{5T}}{(j_{11} - |k|^\theta)E_9 + j_{12}},\\
a_T &= 2(\beta A^*)^3|\zeta_1|^2 + \beta(\zeta_1 + \bar{\zeta}_1),\\
b_T &= -\alpha(\zeta_1 + \bar{\zeta}_1),\\
a_H &= 2(\beta A^*)^3|\eta_1|^2 + \beta(\eta_1 + \bar{\eta}_1),\\
b_H &= -\alpha(\eta_1 + \bar{\eta}_1),\\
a_{2T} &= (\beta A^*)^3\zeta_1^2 + \beta\zeta_1,\\
b_{2T} &= -\alpha\zeta_1,\\
a_{3T} &= a_T,\\
b_{3T} &= b_T,\\
a_{4H} &= a_{2T},\\
b_{4H} &= b_{2T},\\
a_{5T} &= 2(\beta A^*)^3\zeta_1\bar{\eta}_1 + \beta(\zeta_1 + \bar{\eta}_1),\\
b_{5T} &= -\alpha(\zeta_1 + \bar{\eta}_1).
\end{aligned}$$

To solve the $\mathcal{O}\left(\varepsilon^3\right)$ equation, the Fredholm solubility condition requires the right-hand side vector to be orthogonal to the null eigenvector of the adjoint operator $L_c^\dagger$. The null eigenvector associated with the Turing bifurcation is $\binom{\zeta_1^*}{\zeta_2^*}e^{-ik_j\cdot x}$, where

$$\zeta^* = \begin{pmatrix}\zeta_1^*\\ \zeta_2^*\end{pmatrix} = \begin{pmatrix}1\\ \frac{d_1k^\theta - \beta A^*(1-\beta A^*)}{-\alpha^* A^*}\end{pmatrix},$$

and for the Hopf bifurcation, it is $\binom{\eta_1^*}{\eta_2^*}e^{-i\omega_c t}$, where

$$\eta^* = \begin{pmatrix}\eta_1^*\\ \eta_2^*\end{pmatrix} = \begin{pmatrix}1\\ \frac{\beta A^*(1-\beta A^*)}{\alpha^* A^*}\end{pmatrix}.$$

$L_c^\dagger$ denotes the adjoint of $L_c\left(k^\theta\right)$ for Turing modes and of $L_c(0)$ for Hopf modes.

The orthogonality conditions for the $\mathcal{O}\left(\varepsilon^3\right)$ equation are:

$$\begin{aligned}
\begin{pmatrix}\zeta_1^* & \zeta_2^*\end{pmatrix}e^{-ik_j\cdot r}\cdot\left[L_c\begin{pmatrix}M_3\\ A_3\end{pmatrix}\right] &= 0,\\
\begin{pmatrix}\eta_1^* & \eta_2^*\end{pmatrix}e^{-i\omega_c t}\cdot\left[L_c\begin{pmatrix}M_3\\ A_3\end{pmatrix}\right] &= 0.
\end{aligned}$$

Applying these conditions yields the amplitude equation for the Turing mode W_1:

$$\begin{aligned}
\tilde{\tau}\frac{\partial W_1}{\partial T_2} =& \tilde{\mu}W_1 + \nu\left(\overline{V_2W_3} + \overline{V_3W_2}\right)\\
&+ \left(\xi_1'\left|W_1\right|^2 + \xi_2'\left(\left|W_2\right|^2 + \left|W_3\right|^2\right)\right)W_1\\
&+ \xi_3'|B|^2W_1,
\end{aligned}$$

with coefficients defined as

$$\begin{aligned}
\tilde{\tau} =& \zeta_1\zeta_1^* + \zeta_2\zeta_2^*,\\
\tilde{\mu} =& \zeta_2^*\zeta_1\alpha^{(2)}j_{21}/\alpha + \zeta_2\left(\zeta_2^*\alpha^{(2)}j_{22}/\alpha + \zeta_2^*d_2^{(2)}k^\theta j_{22}/\alpha\right),\\
\nu =& \zeta_1^*\left(2a_1\zeta_1^2 + a_2\zeta_1\zeta_2 + 2a_3\zeta_2^2\right)\\
&+ \zeta_1^*\left(2b_1\zeta_1^2 + b_2\zeta_1\zeta_2 + 2b_3\zeta_2^2\right),\\
\xi_1' =& \left(E_{1T}E_{2T} + E_3E_4\right)\left[\zeta_1^*\left(2a_1\zeta_1 + a_2\zeta_2\right)\right.\\
&\left.+\zeta_2^*\left(2b_1\zeta_1 + b_2\zeta_2\right)\right]\\
&+ \left(E_{2T} + E_4\right)\left[\zeta_1^*\left(a_2\zeta_1 + 2a_3\zeta_2\right)\right.\\
&\left.+\zeta_2^*\left(b_2\zeta_1 + 2b_3\zeta_2\right)\right] + 3a_4\zeta_1^3,\\
\xi_2' =& \left(E_{1T}E_{2T} + E_3E_4\right)\left[\zeta_1^*\left(2a_1\zeta_1 + a_2\zeta_2\right)\right.\\
&\left.+\zeta_2^*\left(2b_1\zeta_1 + b_2\zeta_2\right)\right] + \left(E_{2T} + E_6\right)\left[\zeta_1^*\left(a_2\zeta_1 + 2a_3\zeta_2\right)\right.\\
&\left.+\zeta_2^*\left(b_2\zeta_1 + 2b_3\zeta_2\right)\right] + 6a_4\zeta_1^3,\\
\xi_3' =& \left[2\zeta_1^*\left(a_1\zeta_1 + a_3\zeta_2\right) + 2\zeta_2^*\left(b_1\zeta_1 + b_3\zeta_2\right)\right]E_{1H}E_{2H}\\
&+ \left[\zeta_1^*a_2\left(\zeta_1 + \zeta_2\right) + \zeta_2^*b_2\left(\zeta_1 + \zeta_2\right)\right]E_{2H}\\
&+ 6\left(\zeta_1^*a_4 + \zeta_2^*b_4\right)\zeta_1\left|\eta_1\right|^2,
\end{aligned}$$

and $a_1 = (\beta A^*)^3, a_2 = \beta, a_3 = 0, a_4 = -(\beta A^*)^4, b_1 = 0, b_2 = -\alpha, b_3 = 0, b_4 = 0$. Equations for W_2 and

W_3 are obtained analogously by cyclic permutation of indices.

Relating the amplitudes back to the original variables using (27) and (26),

$$
\begin{aligned}
Z_j &= \begin{pmatrix} Z_j^M \\ Z_j^A \end{pmatrix} = \begin{pmatrix} \zeta_1 \\ \zeta_2 \end{pmatrix} (\varepsilon W_j + \varepsilon^2 V_j + \mathcal{O}\left(\varepsilon^3\right)), \\
\begin{pmatrix} B^M \\ B^A \end{pmatrix} &= \begin{pmatrix} \eta_1 \\ \eta_2 \end{pmatrix} \varepsilon \mathcal{H}, \\
\frac{\partial Z_j^M}{\partial t} &= \varepsilon^3 \zeta_1 \frac{\partial W_j}{\partial T_2} + \mathcal{O}\left(\varepsilon^4\right), \quad j = 1, 2, 3, \\
\frac{\partial B^M}{\partial t} &= \varepsilon^3 \eta_1 \frac{\partial B}{\partial T_2} + \mathcal{O}\left(\varepsilon^4\right),
\end{aligned}
$$

and substituting into the amplitude equation for W_1 gives the evolution for Z_1^M:

$$
\begin{aligned}
\frac{\partial Z_1^M}{\partial t} =& \mu Z_1^M + h\overline{Z_2^M Z_3^M} + (\xi_1 \left|Z_1^M\right|^2 \\
&+ \xi_2 \left(\left|Z_2^M\right|^2 + \left|Z_3^M\right|^2\right)) Z_1^M + \xi_3 \left|B^M\right|^2 Z_1^M.
\end{aligned}
$$

The coefficients are rescaled as

$$
\begin{aligned}
h &= \frac{\nu}{\tau_0 \zeta_1}, \quad \xi_1 = \frac{\xi_1'}{\tau_0 \zeta_1^2}, \quad \xi_2 = \frac{\xi_2'}{\tau_0 \zeta_1^2}, \quad \xi_3 = \frac{\xi_3'}{\tau_0 \eta_1^2}, \\
\mu &= \left[\zeta_1 \zeta_2^* \frac{(\alpha - \alpha^*) j_{21}}{\alpha} \right. \\
&\left. + \zeta_2 \left(\zeta_2^* \frac{(\alpha - \alpha^*) j_{22}}{\alpha} + \zeta_2^* k^\theta \frac{(d_2 - d_2^*) j_{22}}{\alpha}\right)\right] / \tau_0.
\end{aligned}
$$

Similarly, the amplitude equation for the Hopf mode $\mathcal{H}$ is derived

$$
\begin{aligned}
\tau \frac{\partial \mathcal{H}}{\partial T_2} =& \zeta_1 \eta_2^* \alpha^{(2)} j_{21} / \alpha \mathcal{H} + \xi_{01}' \left|\mathcal{H}\right|^2 \mathcal{H} \\
&+ \xi_{02}' \left(\left|W_1\right|^2 + \left|W_2\right|^2 + \left|W_3\right|^2\right) \mathcal{H},
\end{aligned}
$$

where

$$
\begin{aligned}
\tau &= \zeta_1 \eta_1^* + \zeta_2 \eta_2^*, \\
\xi_{01}' &= \eta_1^* \left[\left(2a_1 \bar{\eta}_1 + a_2 \bar{\eta}_2\right) E_7 E_8 + \left(a_2 \bar{\eta}_1 + 2a_3 \bar{\eta}_2\right) E_8 \right. \\
&\left. + 3a_4 |\eta_1|^2 \eta_1\right] \\
&+ \eta_2^* \left[\left(2b_1 \bar{\eta}_1 + b_2 \bar{\eta}_2\right) E_7 E_8 + \left(b_2 \bar{\eta}_1 + 2b_3 \bar{\eta}_2\right) E_8 \right. \\
&\left. + 3b_4 |\eta_1|^2 \eta_1\right], \\
\xi_{02}' &= \eta_1^* \left[\left(2a_1 \bar{\zeta}_1 + a_2 \bar{\zeta}_2\right) E_9 E_{10} + \left(a_2 \bar{\zeta}_1 + 2a_3 \bar{\zeta}_2\right) E_{10} \right. \\
&\left. + 6a_4 |\zeta_1|^2 \eta_1\right] \\
&+ \eta_2^* \left[\left(2b_1 \bar{\zeta}_1 + b_2 \bar{\zeta}_2\right) E_9 E_{10} + \left(b_2 \bar{\zeta}_1 + 2b_3 \bar{\zeta}_2\right) E_{10} \right. \\
&\left. + 6b_4 |\zeta_1|^2 \eta_1\right].
\end{aligned}
$$

Expressed in terms of B^M and Z_j^M, this becomes

$$
\begin{aligned}
\frac{\partial B^M}{\partial t} =& \sigma B^M + \xi_{01} \left|B^M\right|^2 B^M \\
&+ \xi_{02} \left(\left|Z_1^M\right|^2 + \left|Z_2^M\right|^2 + \left|Z_3^M\right|^2\right) B^M,
\end{aligned}
$$

with coefficients

$$
\begin{aligned}
\sigma &= \frac{\zeta_1 \eta_2^* (\alpha - \alpha^*) j_{21} / \alpha}{\tau}, \\
\xi_{01} &= \frac{\xi_{01}'}{\tau \eta_1^2}, \\
\xi_{02} &= \frac{\xi_{02}'}{\tau \zeta_1^2}.
\end{aligned}
$$

Thus, the complete coupled set of amplitude equations governing the interaction between one Hopf mode and three Turing modes with mutually orthogonal wave vectors is obtained:

$$
\begin{aligned}
\frac{\partial B^M}{\partial t} &= \sigma B^M + \xi_{01} |B^M|^2 B^M \\
&\quad + \xi_{02} \left(|Z_1^M|^2 + |Z_2^M|^2 + |Z_3^M|^2\right) B^M, \\
\frac{\partial Z_1^M}{\partial t} &= \mu Z_1^M + h\overline{Z_2^M Z_3^M} + \left(\xi_1 |Z_1^M|^2 + \xi_2 \left(|Z_2^M|^2 \right.\right. \\
&\quad \left.\left. + |Z_3^M|^2\right)\right) Z_1^M + \xi_3 |B^M|^2 Z_1^M, \\
\frac{\partial Z_2^M}{\partial t} &= \mu Z_2^M + h\overline{Z_3^M Z_1^M} + \left(\xi_1 |Z_2^M|^2 \right. \\
&\quad \left. + \xi_2 \left(|Z_1^M|^2 + |Z_3^M|^2\right)\right) Z_2^M + \xi_3 |B^M|^2 Z_2^M, \\
\frac{\partial Z_3^M}{\partial t} &= \mu Z_3^M + h\overline{Z_1^M Z_2^M} + \left(\xi_1 |Z_3^M|^2 \right. \\
&\quad \left. + \xi_2 \left(|Z_1^M|^2 + |Z_2^M|^2\right)\right) Z_3^M + \xi_3 |B^M|^2 Z_3^M.
\end{aligned} \tag{28}
$$

The amplitude equations (28) describing the coupled dynamics of the Hopf mode and the three orthogonal Turing modes are now established. To determine the resultant spatiotemporal patterns, the subsequent analysis will focus on identifying the equilibrium points of these amplitude equations and assessing their stability.

In Equation (28), each complex amplitude can be expressed in polar form with moduli $\rho_j = \left|Z_j^M\right|$, $\phi = |B^M|$ and phase angles φ_j, $\Delta\omega$. Substituting $Z_j^M = \rho_j \exp(i\varphi_j)$ and $B^M = \mathfrak{B} \exp(i\Delta\omega t)$ into Eq. (28) and isolating real and imaginary components

yields:

$$\begin{aligned}
\frac{\partial \varphi}{\partial t} &= -h\frac{\rho_1^2\rho_2^2+\rho_1^2\rho_3^2+\rho_3^2\rho_2^2}{\rho_1\rho_2\rho_3}\sin\varphi,\\
\frac{\partial \rho_1}{\partial t} &= \mu\rho_1 + h\rho_2\rho_3\cos\varphi\\
&\quad + \left(\xi_1\rho_1^2+\xi_2\rho_2^2+\xi_3\rho_3^2\right)\rho_1 + \xi_3|\mathfrak{B}|^2\rho_1,\\
\frac{\partial \rho_2}{\partial t} &= \mu\rho_2 + h\rho_1\rho_3\cos\varphi\\
&\quad + \left(\xi_1\rho_2^2+\xi_2\rho_1^2+\xi_3\rho_3^2\right)\rho_2 + \xi_3|\mathfrak{B}|^2\rho_2,\\
\frac{\partial \rho_3}{\partial t} &= \mu\rho_3 + h\rho_1\rho_2\cos\varphi\\
&\quad + \left(\xi_1\rho_3^2+\xi_2\rho_2^2+\xi_3\rho_1^2\right)\rho_3 + \xi_3|\mathfrak{B}|^2\rho_3,\\
\frac{\partial \mathfrak{B}}{\partial t} &= \sigma\mathfrak{B} + \mathrm{Re}\,\xi_{01}|\mathfrak{B}|^2\mathfrak{B} + \mathrm{Re}\,\xi_{02}\left(\rho_1^2+\rho_2^2+\rho_3^2\right)\mathfrak{B},\\
\Delta\omega &= \mathrm{Im}\,\xi_{01}|\mathfrak{B}|^2 + \mathrm{Im}\,\xi_{02}\left(\rho_1^2+\rho_2^2+\rho_3^2\right),
\end{aligned} \tag{29}$$

where $\varphi = \sum_{j=1}^{3}\varphi_j$. Analysis of system (28) reveals that stationary states require the phase to stabilize at $\varphi = 0$ or $\varphi = \pi$. Given non-negative moduli $\rho_i \geq 0\,(i = 1, 2, 3)$, the solution $\varphi = 0$ is stable for $h > 0$, whereas $\varphi = \pi$ is stable for $h < 0$.

Pattern formation necessitates phase stability, leading to the reduced amplitude equations:

$$\begin{aligned}
\frac{\partial \rho_1}{\partial t} &= \mu\rho_1 + |h|\rho_2\rho_3\\
&\quad + \left(\xi_1\rho_1^2+\xi_2\rho_2^2+\xi_3\rho_3^2\right)\rho_1 + \xi_3|\mathfrak{B}|^2\rho_1,\\
\frac{\partial \rho_2}{\partial t} &= \mu\rho_2 + |h|\rho_1\rho_3\\
&\quad + \left(\xi_1\rho_2^2+\xi_2\rho_1^2+\xi_3\rho_3^2\right)\rho_2 + \xi_3|\mathfrak{B}|^2\rho_2,\\
\frac{\partial \rho_3}{\partial t} &= \mu\rho_3 + |h|\rho_1\rho_2\\
&\quad + \left(\xi_1\rho_3^2+\xi_2\rho_2^2+\xi_3\rho_1^2\right)\rho_3 + \xi_3|\mathfrak{B}|^2\rho_3,\\
\frac{\partial \mathfrak{B}}{\partial t} &= \sigma\mathfrak{B} + \mathrm{Re}\,\xi_{01}|\mathfrak{B}|^2\mathfrak{B}\\
&\quad + \mathrm{Re}\,\xi_{02}\left(\rho_1^2+\rho_2^2+\rho_3^2\right)\mathfrak{B}.
\end{aligned} \tag{30}$$

Theorem 2. Consider the reduced amplitude equations (30) derived from the weakly nonlinear analysis of the superdiffusive mussel-algae system (4) at the Turing-Hopf bifurcation point. The system (4) admits two typical classes of pattern solutions in the neighborhood of the Turing-Hopf bifurcation point, and their existence and asymptotic stability conditions are given as follows:

1. **Spatiotemporal periodic pattern** Let $\rho_2 = \rho_3 = 0$, the spatiotemporal periodic pattern of system (4) has the moduli of the amplitudes satisfying:

$$\rho_1 = \sqrt{\frac{\sigma\xi_3 - \mu\,\mathrm{Re}\,\xi_{01}}{\xi_1\,\mathrm{Re}\,\xi_{01} - \xi_3\,\mathrm{Re}\,\xi_{02}}},$$

$$|\mathfrak{B}| = \sqrt{\frac{\mu\,\mathrm{Re}\,\xi_{02} - \xi_1\sigma}{\xi_1\,\mathrm{Re}\,\xi_{01} - \xi_3\,\mathrm{Re}\,\xi_{02}}}.$$

The spatiotemporal periodic pattern exists if and only if the non-negativity conditions of the moduli hold:

$$\sigma\xi_3 - \mu\,\mathrm{Re}\,\xi_{01} \geq 0, \quad \mu\,\mathrm{Re}\,\xi_{02} - \xi_1\sigma \geq 0.$$

The pattern is asymptotically stable when the denominator of the modulus expressions satisfies:

$$\xi_1\,\mathrm{Re}\,\xi_{01} - \xi_3\,\mathrm{Re}\,\xi_{02} > 0.$$

2. **Hexagonal pattern** Let $\rho_1 = \rho_2 = \rho_3 = \rho$ (spatial symmetry of hexagonal pattern), the hexagonal pattern of system (4) has the moduli of the amplitudes satisfying:

$$\rho = \frac{|h| + \sqrt{|h|^2 - 4\left(\xi_1 + 2\xi_2 - 3\frac{\xi_3\,\mathrm{Re}\,\xi_{02}}{\mathrm{Re}\,\xi_{01}}\right)\left(\mu - \frac{\sigma\xi_3}{\mathrm{Re}\,\xi_{01}}\right)}}{2\left(\xi_1 + 2\xi_2 - 3\frac{\xi_3\,\mathrm{Re}\,\xi_{02}}{\mathrm{Re}\,\xi_{01}}\right)},$$

$$|\mathfrak{B}|^2 = \frac{\sigma + 3\,\mathrm{Re}\,\xi_{02}\rho^2}{\mathrm{Re}\,\xi_{01}}.$$

The hexagonal pattern exists and is asymptotically stable if and only if the following conditions are simultaneously satisfied:

$$2\,\mathrm{Re}\,\xi_{01}|\mathfrak{B}|^2 + 3|h|\rho + 6\left(\xi_1 + 2\xi_2\right)\rho^2 < 0,$$

$$\xi_1 + 2\xi_2 - 3\frac{\xi_3\,\mathrm{Re}\,\xi_{02}}{\mathrm{Re}\,\xi_{01}} > 0,$$

$$|h|^2 > 4\left(\xi_1 + 2\xi_2 - 3\frac{\xi_3\,\mathrm{Re}\,\xi_{02}}{\mathrm{Re}\,\xi_{01}}\right)\left(\mu - \frac{\sigma\xi_3}{\mathrm{Re}\,\xi_{01}}\right),$$

$$\frac{\sigma + 3\,\mathrm{Re}\,\xi_{02}\rho^2}{\mathrm{Re}\,\xi_{01}} > 0.$$

Proof. The proof is based on the stationary state condition of the reduced amplitude equations (30): for a pattern solution to be observable in the system, the time derivatives of the amplitude moduli must vanish at the steady state, i.e., $\frac{\partial\rho_1}{\partial t} = \frac{\partial\rho_2}{\partial t} = \frac{\partial\rho_3}{\partial t} = \frac{\partial\mathfrak{B}}{\partial t} = 0$. We verify the two pattern solutions separately by substituting the symmetry conditions into Eq. (30) and solving the resulting algebraic system.

1) Proof for spatiotemporal periodic pattern ($\rho_2 = \rho_3 = 0$)

Substitute the symmetry condition $\rho_2 = \rho_3 = 0$ into the reduced amplitude equations (30), the system is simplified to a two-variable algebraic system for ρ_1 and $\mathfrak{B}$:

$$0 = \mu\rho_1 + \left(\xi_1\rho_1^2\right)\rho_1 + \xi_3|\mathfrak{B}|^2\rho_1, \tag{30-1}$$

$$0 = \sigma\mathfrak{B} + \operatorname{Re}\xi_{01}|\mathfrak{B}|^2\mathfrak{B} + \operatorname{Re}\xi_{02}\rho_1^2\mathfrak{B}. \tag{30-2}$$

Since the pattern solution is non-trivial ($\rho_1 \neq 0, \mathfrak{B} \neq 0$), we can divide both sides of Eq. (30-1) by ρ_1 and Eq. (30-2) by $\mathfrak{B}$, yielding the **non-trivial steady state equations**:

$$\mu + \xi_1\rho_1^2 + \xi_3|\mathfrak{B}|^2 = 0, \tag{1-1}$$

$$\sigma + \operatorname{Re}\xi_{01}|\mathfrak{B}|^2 + \operatorname{Re}\xi_{02}\rho_1^2 = 0. \tag{1-2}$$

Treat Eqs. (1-1) and (1-2) as a linear system with respect to ρ_1^2 and $|\mathfrak{B}|^2$. We write it in matrix form:

$$\begin{pmatrix} \xi_1 & \xi_3 \\ \operatorname{Re}\xi_{02} & \operatorname{Re}\xi_{01} \end{pmatrix} \begin{pmatrix} \rho_1^2 \\ |\mathfrak{B}|^2 \end{pmatrix} = \begin{pmatrix} -\mu \\ -\sigma \end{pmatrix}.$$

Solve this linear system using **Cramer's rule**. The determinant of the coefficient matrix is:

$$\Delta = \xi_1 \operatorname{Re}\xi_{01} - \xi_3 \operatorname{Re}\xi_{02}.$$

For a unique real solution to exist, $\Delta \neq 0$. Calculating the cofactors and solving for ρ_1^2 and $|\mathfrak{B}|^2$:

$$\rho_1^2 = \frac{1}{\Delta}\begin{vmatrix} -\mu & \xi_3 \\ -\sigma & \operatorname{Re}\xi_{01} \end{vmatrix} = \frac{\sigma\xi_3 - \mu\operatorname{Re}\xi_{01}}{\Delta},$$

$$|\mathfrak{B}|^2 = \frac{1}{\Delta}\begin{vmatrix} \xi_1 & -\mu \\ \operatorname{Re}\xi_{02} & -\sigma \end{vmatrix} = \frac{\mu\operatorname{Re}\xi_{02} - \xi_1\sigma}{\Delta}.$$

Since $\rho_1 = \sqrt{\rho_1^2}$ and $|\mathfrak{B}| = \sqrt{|\mathfrak{B}|^2}$ are moduli of complex amplitudes (non-negative real numbers), their radicands must be non-negative, which gives the existence conditions:

$$\sigma\xi_3 - \mu\operatorname{Re}\xi_{01} \geq 0, \quad \mu\operatorname{Re}\xi_{02} - \xi_1\sigma \geq 0.$$

For asymptotic stability, the denominator $\Delta > 0$ (a necessary condition for the steady state to be a stable node in the amplitude modulus phase plane), which completes the proof for the spatiotemporal periodic pattern.

2) Proof for hexagonal pattern ($\rho_1 = \rho_2 = \rho_3 = \rho$)

The hexagonal pattern is a spatially symmetric pattern with $\rho_1 = \rho_2 = \rho_3 = \rho$, which is a direct consequence of the three mutually orthogonal Turing modes in the 2D spatial domain. Substitute $\rho_1 = \rho_2 = \rho_3 = \rho$ into the reduced amplitude equations (30), the system is simplified by spatial symmetry:

$$0 = \mu\rho + |h|\rho^2 + \left(\xi_1\rho^2 + 2\xi_2\rho^2\right)\rho + \xi_3|\mathfrak{B}|^2\rho, \tag{30-3}$$

$$0 = \sigma\mathfrak{B} + \operatorname{Re}\xi_{01}|\mathfrak{B}|^2\mathfrak{B} + \operatorname{Re}\xi_{02}\cdot 3\rho^2\mathfrak{B}. \tag{30-4}$$

Again, the pattern is non-trivial ($\rho \neq 0, \mathfrak{B} \neq 0$), so divide Eq. 30-3 by ρ and Eq. (30-4) by $\mathfrak{B}$:

$$\mu + |h|\rho + (\xi_1 + 2\xi_2)\rho^2 + \xi_3|\mathfrak{B}|^2 = 0, \tag{2-1}$$

$$\sigma + \operatorname{Re}\xi_{01}|\mathfrak{B}|^2 + 3\operatorname{Re}\xi_{02}\rho^2 = 0. \tag{2-2}$$

First, solve Eq. (2-2) for $|\mathfrak{B}|^2$ (algebraic rearrangement):

$$|\mathfrak{B}|^2 = \frac{\sigma + 3\operatorname{Re}\xi_{02}\rho^2}{\operatorname{Re}\xi_{01}}.$$

This is the expression for $|\mathfrak{B}|^2$ in the theorem, and the non-negativity of the modulus gives the condition $\frac{\sigma+3\operatorname{Re}\xi_{02}\rho^2}{\operatorname{Re}\xi_{01}} > 0$.

Substitute the above expression for $|\mathfrak{B}|^2$ into Eq. (2-1):

$$\mu + |h|\rho + (\xi_1 + 2\xi_2)\rho^2 + \xi_3 \cdot \frac{\sigma + 3\operatorname{Re}\xi_{02}\rho^2}{\operatorname{Re}\xi_{01}} = 0.$$

Combine like terms for ρ^2 and rearrange the equation into a quadratic equation in ρ:

$$\left(\xi_1 + 2\xi_2 - 3\frac{\xi_3\operatorname{Re}\xi_{02}}{\operatorname{Re}\xi_{01}}\right)\rho^2 + |h|\rho + \left(\mu - \frac{\sigma\xi_3}{\operatorname{Re}\xi_{01}}\right) = 0. \tag{2-3}$$

Let $A = \xi_1 + 2\xi_2 - 3\frac{\xi_3\operatorname{Re}\xi_{02}}{\operatorname{Re}\xi_{01}}$, $B = |h|$, $C = \mu - \frac{\sigma\xi_3}{\operatorname{Re}\xi_{01}}$, then Eq. (2-3) is $A\rho^2 + B\rho + C = 0$. For a positive real solution of ρ (modulus is positive), the quadratic equation must satisfy: 1. Discriminant $\Delta = B^2 - 4AC > 0$ (two distinct real roots), i.e.,

$$|h|^2 > 4\left(\xi_1 + 2\xi_2 - 3\frac{\xi_3\operatorname{Re}\xi_{02}}{\operatorname{Re}\xi_{01}}\right)\left(\mu - \frac{\sigma\xi_3}{\operatorname{Re}\xi_{01}}\right);$$

2. Coefficient $A > 0$ (ensures the positive root via Vieta's formulas, since $B = |h| > 0, AC < 0$ from $\Delta > 0$).

Using the quadratic formula to solve for the positive real root of ρ:

$$\rho = \frac{-B + \sqrt{B^2 - 4AC}}{2A} = \frac{|h| + \sqrt{|h|^2 - 4AC}}{2A}$$

(the negative root is discarded because $\rho > 0$).

Finally, the asymptotic stability condition $2\,\mathrm{Re}\,\xi_{01}|\mathfrak{B}|^2 + 3|h|\rho + 6\,(\xi_1 + 2\xi_2)\,\rho^2 < 0$ is derived from the linear stability analysis of the steady state $(\rho, |\mathfrak{B}|)$: we linearize the reduced amplitude equations (30) around the steady state, compute the Jacobian matrix of the linearized system, and require all eigenvalues to have negative real parts (a necessary and sufficient condition for asymptotic stability). This yields the aforementioned inequality, which completes the proof for the hexagonal pattern. □

Remark 2. When $\mathfrak{B} = 0$, system (28) simplifies to the scenario of Turing instability (or Turing bifurcation) in system (4), as comprehensively analyzed in [41]. Conversely, under the condition $\rho_1 = \rho_2 = \rho_3 = 0$, system (28) reduces to the Hopf bifurcation case of system (4). In these two limiting scenarios, the respective bifurcations induce either spatially nonhomogeneous patterns or temporally periodic solutions. However, during a Turing-Hopf bifurcation , spatiotemporally nonhomogeneous dynamics may emerge, exhibiting complex spatiotemporal patterns.

Remark 3. Weakly nonlinear analysis is a perturbative method valid in a small neighborhood of the bifurcation point, where the amplitudes of unstable modes are small. It expands the solution in powers of a small parameter ε and yields universal amplitude equations that govern pattern selection and stability near onset. Its strength is analytical tractability and predictive power for codimension-one/two bifurcations. Strongly nonlinear analysis, by contrast, applies far from the bifurcation threshold where amplitudes are no longer small and perturbation expansions diverge. It typically requires global bifurcation theory, numerical continuation, or direct simulation, and generally does not yield closed-form normal forms. In this paper, weakly nonlinear analysis is the appropriate tool because we aim to classify the universal spatiotemporal patterns (stripes, hexagons, mixed modes) in the immediate vicinity of the Turing-Hopf point.

4 Numerical simulations

This section provides numerical simulations to validate and extend the analytical results established in Sections 2 and 3. Adopting spatial and temporal discretizations $\Delta x = 1$ and $\Delta t = 0.005$ respectively, we implement the parameter set $\beta = 2.5$, $m = 0.3$, $d_1 = 0.15$, where α and d_2 serve as bifurcation parameters. As derived in Section 3, system (4) possesses a unique interior equilibrium $E^* = (1.1538, 0.2133)$. Initially examining the non-diffusive case, the positive equilibrium E^* exhibits asymptotic stability when $\alpha = 0.115 > \alpha^*$ under initial conditions $(M_0, A_0) = (0.1, 0.1)$. Conversely, when $\alpha = 0.105 < \alpha^*$, a stable limit cycle emerges via bifurcation from the unstable equilibrium E^* with identical initial data. The corresponding phase portraits are detailed in Figures 2 and 3.

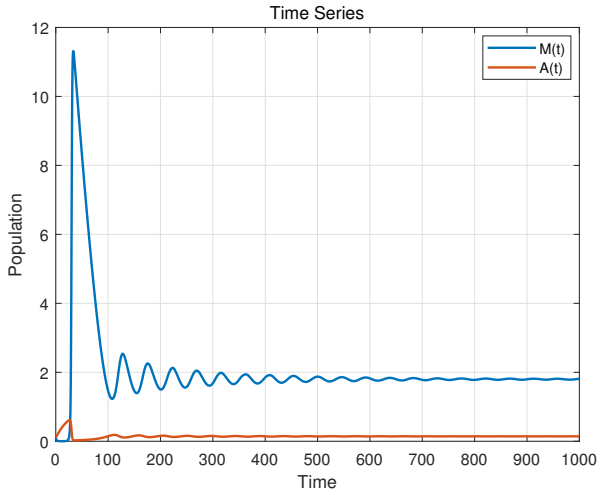

(a)

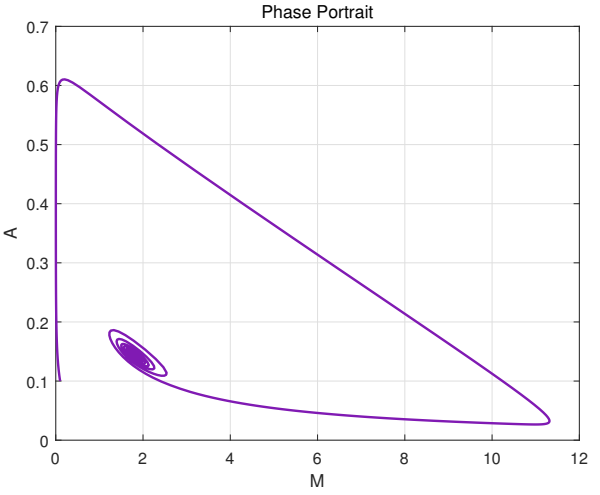

(b)

Figure 2. For system (4) with $(d_1 = d_2 = 0)$, and $\alpha > \alpha^*$, time series and phase portrait show E^* is asymptotically stable.

Subsequently, we explore dynamical patterns proximal to the Turing-Hopf bifurcation point. Parameterized with $\beta = 2.5$, $m = 0.3$, $d_1 = 0.15$, and $t = 500$, with initial values (M_0, A_0) chosen as $(M^* + 0.001(\cos(x) +$

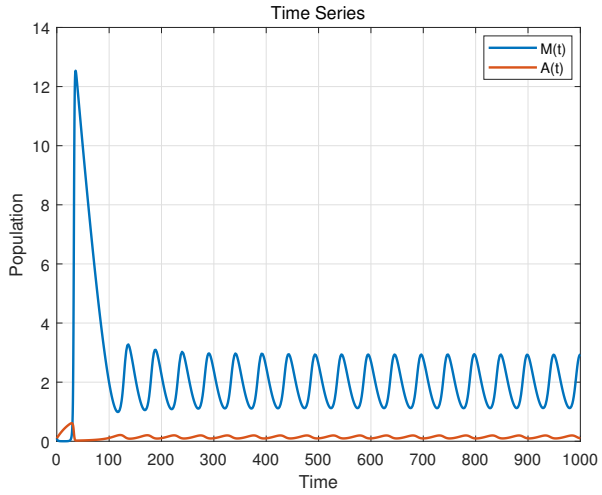

(a)

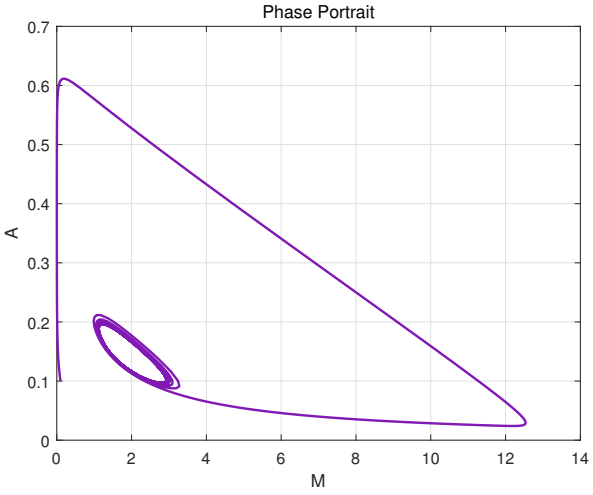

(b)

Figure 3. For system (4) with $(d_1 = d_2 = 0)$, and $\alpha < \alpha^*$, time series and phase portrait show that a stable limit cycle bifurcates from E^*.

$\cos(y)), A^* + 0.001(\cos(x) + \cos(y)))$, where α and d_2 constitute variable bifurcation parameters, the bifurcation point is readily verified as $(d_2^*, \alpha^*) = (0.6538, 0.1093)$.

When selecting parameters at criticality ($d_2 = d_2^*$, $\alpha = \alpha^*$) or within its neighborhood, these values satisfy the existence conditions for spatiotemporally periodic solutions. These solutions manifest as either stripe patterns or hybrid stripe-spot configurations, as visualized in Figures 4 and 5. Numerical evidence further indicates that reducing the fractional order exponent θ induces a morphological transition from stripes to composite stripe-spot patterns, accompanied by the emergence of secondary bifurcations.

When selecting parameter values $(d_2, \alpha) = (0.1, 0.05)$ within region R3, solutions exhibiting hexagonal-like

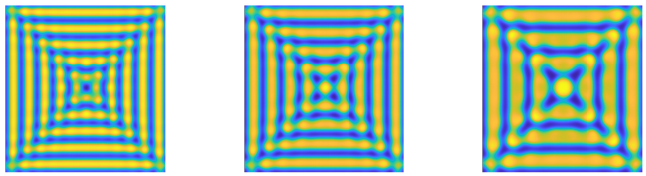

(a) $\theta = 2$ (b) $\theta = 1.5$ (c) $\theta = 1.1$

Figure 4. Under critical parameter conditions $d_2 = d_2^*$ and $\alpha = \alpha^*$, the emergent mussel density patterns (M) are presented in panels (a), (b), and (c) for $\theta = 2, 1.5$, and 1.1 respectively.

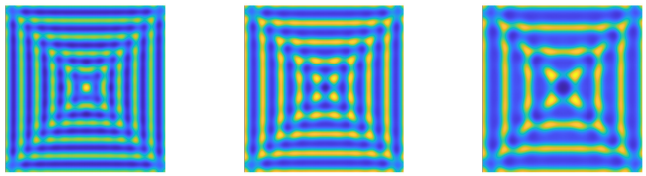

(a) $\theta = 2$ (b) $\theta = 1.5$ (c) $\theta = 1.1$

Figure 5. Under critical parameter conditions $d_2 = d_2^*$ and $\alpha = \alpha^*$, the emergent algae density patterns (A) are presented in panels (a), (b), and (c) for $\theta = 2, 1.5$, and 1.1 respectively.

patterns emerge. Numerical simulations reveal that pattern morphologies remain qualitatively similar under decreasing fractional order θ, as documented in Figures 6 and 7.

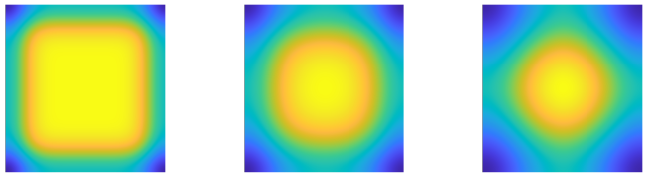

(a) $\theta = 2$ (b) $\theta = 1.5$ (c) $\theta = 1.1$

Figure 6. When $d_2 = 0.1 < d_2^*$ and $\alpha = 0.05 < \alpha^*$, the emergent mussel density patterns (M) are presented in panels (a), (b), and (c) for $\theta = 2, 1.5$, and 1.1 respectively.

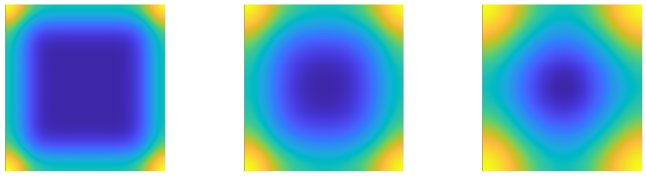

(a) $\theta = 2$ (b) $\theta = 1.5$ (c) $\theta = 1.1$

Figure 7. When $d_2 = 0.1 < d_2^*$ and $\alpha = 0.05 < \alpha^*$, the emergent algae density patterns (A) are presented in panels (a), (b), and (c) for $\theta = 2, 1.5$, and 1.1 respectively.

For the parameter configuration $(d_2, \alpha) = (3, 0.05)$

situated within region R4 at a significant distance from the critical bifurcation point (d_2^*, α^*) these values fulfill the existence criteria for spatiotemporally periodic solutions. Numerical simulations reveal that a gradual decrement in the fractional order θ precipitates a morphological transition, wherein labyrinthine patterns undergo a progressive transformation toward spot patterns. This evolutionary dynamics of pattern formation is empirically validated through the comparative analysis of Figures 8 and 9.

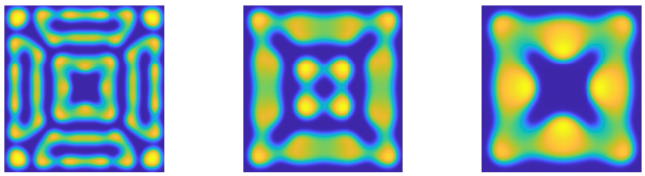

(a) $\theta = 2$ (b) $\theta = 1.5$ (c) $\theta = 1.1$

Figure 8. When $d_2 = 3 > d_2^*$ and $\alpha = 0.05 < \alpha^*$, the emergent mussel density patterns (M) are presented in panels (a), (b), and (c) for $\theta = 2$, 1.5, and 1.1 respectively.

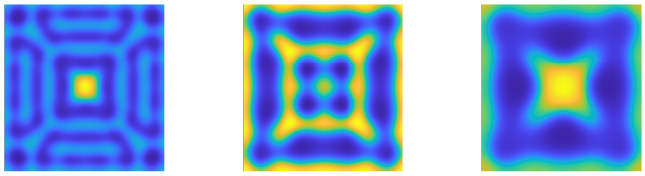

(a) $\theta = 2$ (b) $\theta = 1.5$ (c) $\theta = 1.1$

Figure 9. When $d_2 = 3 > d_2^*$ and $\alpha = 0.05 < \alpha^*$, the emergent algae density patterns (A) are presented in panels (a), (b), and (c) for $\theta = 2$, 1.5, and 1.1 respectively.

These results demonstrate that θ is not merely a mathematical parameter but an ecological control factor: as θ decreases, the superdiffusive Lévy jumps become more prominent, flattening spatial gradients and triggering transitions from regular stripes to disordered spot patterns.

5 Conclusions

This study investigated the impact of superdiffusion on Turing-Hopf bifurcations within a mussel-algae model. We established sufficient conditions that rigorously guarantee the existence of Turing-Hopf bifurcations, and employed a weakly nonlinear analysis to derive the corresponding amplitude equations in the vicinity of the bifurcation point of system (4). Because Turing-Hopf bifurcations are codimension-two, the dimensionless parameter α and diffusion coefficient d_2 serve as the designated bifurcation parameters. These amplitude equations govern the underlying pattern-selection mechanisms, facilitating the classification of spatiotemporal patterns and the analysis of stability. Our main findings reveal that the fractional exponent θ plays a decisive role in pattern morphology: numerical simulations confirm that as θ decreases from 2 toward 1.1, the system undergoes transitions from regular stripes to mixed stripe-spot patterns and eventually to labyrinthine or spot-like patterns, which are unattainable in classical integer-order diffusion models. To our knowledge, this is the first analytical derivation of coupled Turing-Hopf amplitude equations for a spatially fractional reaction-diffusion system; existing studies on fractional reaction-diffusion have addressed either temporal fractional derivatives [27] or spatial fractional Turing instability without Hopf coupling [36, 38, 41], but not the full Turing-Hopf codimension-two scenario under spatial fractional diffusion. The stability criteria for both spatiotemporal periodic and hexagonal patterns are also explicitly established.

Looking ahead, several directions merit further investigation. It would be worthwhile to extend the present framework to models with both temporal and spatial fractional derivatives, to explore higher-codimension bifurcations in enlarged parameter spaces, and to generalize the methodology to multi-species food-web models. Additionally, fitting the fractional exponent θ against empirical mussel-bed imagery would help bridge the gap between theoretical pattern predictions and ecological field observations.

Data Availability Statement

Data will be made available on request.

Funding

This work was supported by the Natural Science Foundation of Xinjiang Uygur Autonomous Region, China under Grant 2025D01C41, and the National Natural Science Foundation of China under Grant 12461097.

Conflicts of Interest

The authors declare no conflicts of interest.

AI Use Statement

The authors declare that no generative AI was used in the preparation of this manuscript.

Ethical Approval and Consent to Participate

Not applicable.

References

[1] Turing, A. M. (1952). The chemical basis of morphogenesis. *Philosophical Transactions of the Royal Society of London. Series B, Biological Sciences, 237*(641), 37-72. [CrossRef]

[2] Ninomiya, H. (2024). Example of Turing instability by equal Diffusion. *Journal of Differential Equations, 392*, 255-265. [CrossRef]

[3] Staddon, M. F. (2024). How the zebra got its stripes: Curvature-dependent diffusion orients Turing patterns on three-dimensional surfaces. *Physical Review E, 110*(3), 034402. [CrossRef]

[4] Bao, X., & Tian, C. (2024). Turing patterns in a networked vegetation model. *Mathematical Biosciences and Engineering, 21*(11), 7601-7620. [CrossRef]

[5] Yang, C. (2025). Turing instabilities analysis of a reaction-diffusion system for malware Propagation on mobile wireless sensor networks. *Physica Scripta, 100*(7), 075222. [CrossRef]

[6] Champagne-Ruel, A., Zakaib-Bernier, S., & Charbonneau, P. (2024). Diffusion and pattern formation in spatial games. *Physical Review E, 110*(1), 014301. [CrossRef]

[7] Tian, S. (2025). Turing Instability of Periodic Solutions and Stationary Patterns Induced by Cross-Diffusion in a Holling Type-II Prey–Predator Model. *International Journal of Bifurcation and Chaos, 35*(09), 2550109. [CrossRef]

[8] Calderón-Barreto, E. A., Bravo-Castillero, J., & Aragón, J. L. (2024). Turing patterns in domains with periodic inhomogeneities; a homogenization approach. *Chaos, Solitons & Fractals, 179*, 114433. [CrossRef]

[9] Torcicollo, I., & Vitiello, M. (2024). Turing instability and spatial pattern formation in a model of urban crime. *Mathematics, 12*(7), 1097. [CrossRef]

[10] Yadav, R., & Sen, M. (2024). Spatio-temporal complexity in a prey-predator system with Holling type-IV response and Leslie-type numerical response: Turing and steady-state bifurcations. *Mathematics and Computers in Simulation, 225*, 283-302. [CrossRef]

[11] Ma, X., Wang, J., Zhu, Y., Wang, Z., & Sun, Y. (2024). Turing–Hopf Bifurcation Coinduced by Diffusion and Delay in Gierer–Meinhardt Systems. *International Journal of Bifurcation and Chaos, 34*(13), 2450162. [CrossRef]

[12] Tian, J., & Liu, P. (2025). Turing-bifurcation in a cross-diffusive predator–prey system with generalist predator and nonlocal terms. *Communications in Nonlinear Science and Numerical Simulation, 147*, 108821. [CrossRef]

[13] Lv, Y. (2024). Turing–Turing bifurcation in an activator–inhibitor system with gene expression time delay. *Communications in Nonlinear Science and Numerical Simulation, 131*, 107836. [CrossRef]

[14] Shen, H., & Song, Y. (2024). Spatiotemporal patterns in a diffusive resource–consumer model with distributed memory and maturation delay. *Mathematics and Computers in Simulation, 221*, 622-644. [CrossRef]

[15] Zhang, J., & Fu, S. (2024). Hopf bifurcation and Turing pattern of a diffusive Rosenzweig-MacArthur model with fear factor. *AIMS Mathematics, 9*(11), 32514-32551. [CrossRef]

[16] Baurmann, M., Gross, T., & Feudel, U. (2007). Instabilities in spatially extended predator–prey systems: Spatio-temporal patterns in the neighborhood of Turing–Hopf bifurcations. *Journal of Theoretical Biology, 245*(2), 220-229. [CrossRef]

[17] van de Koppel, J., Gascoigne, J. C., Theraulaz, G., Rietkerk, M., Mooij, W. M., & Herman, P. M. (2008). Experimental evidence for spatial self-organization and its emergent effects in mussel bed ecosystems. *Science, 322*(5902), 739-742. [CrossRef]

[18] Rovinsky, A., & Menzinger, M. (1992). Interaction of Turing and Hopf bifurcations in chemical systems. *Physical Review A, 46*(10), 6315. [CrossRef]

[19] Song, Y., Zhang, T., & Peng, Y. (2016). Turing–Hopf bifurcation in the reaction–diffusion equations and its applications. *Communications in Nonlinear Science and Numerical Simulation, 33*, 229-258. [CrossRef]

[20] Song, Y., Jiang, H., Liu, Q. X., & Yuan, Y. (2017). Spatiotemporal dynamics of the diffusive Mussel-Algae model near Turing-Hopf bifurcation. *SIAM Journal on Applied Dynamical Systems, 16*(4), 2030-2062. [CrossRef]

[21] Koppel, J. V. D., Rietkerk, M., Dankers, N., & Herman, P. M. (2005). Scale-dependent feedback and regular spatial patterns in young mussel beds. *The American Naturalist, 165*(3), E66-E77. [CrossRef]

[22] Cangelosi, R. A., Wollkind, D. J., Kealy-Dichone, B. J., & Chaiya, I. (2015). Nonlinear stability analyses of Turing patterns for a mussel-algae model. *Journal of Mathematical Biology, 70*(6), 1249-1294. [CrossRef]

[23] Wang, R. H., Liu, Q. X., Sun, G. Q., Jin, Z., & van de Koppel, J. (2008). Nonlinear dynamic and pattern bifurcations in a model for spatial patterns in young mussel beds. *Journal of the Royal Society Interface, 6*(37), 705. [CrossRef]

[24] Humphries, N. E., Queiroz, N., Dyer, J. R., Pade, N. G., Musyl, M. K., Schaefer, K. M., ... & Sims, D. W. (2010). Environmental context explains Lévy and Brownian movement patterns of marine predators. *Nature, 465*(7301), 1066-1069. [CrossRef]

[25] Bouchaud, J. P., & Georges, A. (1990). Anomalous diffusion in disordered media: statistical mechanisms, models and physical applications. *Physics reports, 195*(4-5), 127-293. [CrossRef]

[26] Henry, B. I., & Wearne, S. L. (2002). Existence

of Turing instabilities in a two-species fractional reaction-diffusion system. *SIAM Journal on Applied Mathematics, 62*(3), 870-887. [CrossRef]

[27] Djilali, S., Ghanbari, B., Bentout, S., & Mezouaghi, A. (2020). Turing-Hopf bifurcation in a diffusive mussel-algae model with time-fractional-order derivative. *Chaos, Solitons & Fractals, 138*, 109954. [CrossRef]

[28] Freyberg, D. L. (1986). A natural gradient experiment on solute transport in a sand aquifer: 2. Spatial moments and the advection and dispersion of nonreactive tracers. *Water Resources Research, 22*(13), 2031-2046. [CrossRef]

[29] Adams, E. E., & Gelhar, L. W. (1992). Field study of dispersion in a heterogeneous aquifer: 2. Spatial moments analysis. *Water Resources Research, 28*(12), 3293-3307. [CrossRef]

[30] Metzler, R., & Klafter, J. (2000). The random walk's guide to anomalous diffusion: a fractional dynamics approach. *Physics reports, 339*(1), 1-77. [CrossRef]

[31] Nec, Y. (2012). Spike-Type Solutions to One Dimensional Gierer–Meinhardt Model with Lévy Flights. *Studies in Applied Mathematics, 129*(3), 272-299. [CrossRef]

[32] Sims, D. W., Southall, E. J., Humphries, N. E., Hays, G. C., Bradshaw, C. J., Pitchford, J. W., ... & Metcalfe, J. D. (2008). Scaling laws of marine predator search behaviour. *Nature, 451*(7182), 1098-1102. [CrossRef]

[33] Molz III, F. J., Fix III, G. J., & Lu, S. (2002). A physical interpretation for the fractional derivative in Levy diffusion. *Applied Mathematics Letters, 15*(7), 907-911. [CrossRef]

[34] Cheng, H., & Yuan, R. (2015). The spreading property for a prey-predator reaction-diffusion system with fractional diffusion. *Fractional Calculus and Applied Analysis, 18*(3), 565-579. [CrossRef]

[35] Bendahmane, M., Ruiz-Baier, R., & Tian, C. (2016). Turing pattern dynamics and adaptive discretization for a super-diffusive Lotka-Volterra model. *Journal of mathematical biology, 72*(6), 1441-1465. [CrossRef]

[36] Henry, B. I., Langlands, T. A. M., & Wearne, S. L. (2005). Turing pattern formation in fractional activator-inhibitor systems. *Physical Review E—Statistical, Nonlinear, and Soft Matter Physics, 72*(2), 026101. [CrossRef]

[37] Gafiychuk, V., & Datsko, B. (2008). Stability analysis and limit cycle in fractional system with Brusselator nonlinearities. *Physics Letters A, 372*(29), 4902-4904. [CrossRef]

[38] Langlands, T. A., Henry, B. I., & Wearne, S. L. (2007). Turing pattern formation with fractional diffusion and fractional reactions. *Journal of Physics: Condensed Matter, 19*(6), 065115. [CrossRef]

[39] Viswanathan, G. M., Afanasyev, V., Buldyrev, S. V., Murphy, E. J., Prince, P. A., & Stanley, H. E. (1996). Lévy flight search patterns of wandering albatrosses. *Nature, 381*(6581), 413-415. [CrossRef]

[40] Song, Y., & Zou, X. (2014). Spatiotemporal dynamics in a diffusive ratio-dependent predator–prey model near a Hopf–Turing bifurcation point. *Computers & Mathematics with Applications, 67*(10), 1978-1997. [CrossRef]

[41] Liu, B., Wu, R., Iqbal, N., & Chen, L. (2017). Turing patterns in the Lengyel–Epstein system with superdiffusion. *International Journal of Bifurcation and Chaos, 27*(08), 1730026. [CrossRef]